

Article

Archaeological Ceramic Diagenesis: Clay Mineral Recrystallization in Sherds from a Late Byzantine Kiln, Israel

Steve Weiner ^{*,1}, Alla Nagorsky ², Yishai (Isai) Feldman ³ and Anna Kossoy ³

¹ Kimmel Center for Archaeological Science and the Department of Structural Biology, Weizmann Institute of Science, Rehovot 76100, Israel

² Israel Antiquities Authority, P.O.B. 586, Jerusalem 91004, Israel; allanag31@gmail.com

³ Department of Chemical Research Support, Weizmann Institute of Science, Rehovot 76100, Israel; Isai.Feldman@weizmann.ac.il (Y.(I).F.); anna-eden.kossoy@weizmann.ac.il (A.K.)

* Correspondence: steve.weiner@weizmann.ac.il

Received: 15 March 2020; Accepted: 27 April 2020; Published: 30 April 2020



Abstract: The pseudo-amorphous clay components of some of the pottery sherds that formed a surface in the firing chamber of a Late Byzantine kiln were shown by Fourier Transform Infrared Spectroscopy to have undergone almost complete recrystallization. Powder X-ray diffraction showed that the crystalline montmorillonite component of these sherds increased and kaolinite formed de novo. As this recrystallization process only occurred in the center of the firing chamber, we infer that the recrystallization process was due to repeated exposure of the sherds to high temperatures. The zeolite gonnardite was identified by X-ray diffraction. The chemical compositions of sodium-rich minerals, determined by energy dispersive X-ray spectroscopy (EDS), are consistent with the presence of gonnardite and analcime, and showed that the sodium was partially substituted by calcium and other cations. As these zeolites were also present in sherds from the upper pottery chamber, they did not form only as a result of repeated exposure to high temperatures. The demonstration that the clay mineral component of ceramics can undergo diagenetic recrystallization supports the possibility that provenience studies based on elemental analyses, especially of cooking pots that are repeatedly exposed to high temperatures, may be affected by recrystallization.

Keywords: pseudo-amorphous clays; archaeological ceramics; authigenic minerals; zeolites; recrystallization

1. Introduction

Traditional ceramics are usually formed by heating clay mixed with added inorganic temper such as quartz and calcite, as well as organic temper, to temperatures ranging from around 600 to 1000 °C for hours or even days [1–4]. The clay and calcite mineral components undergo major phase transformations and reactions due to the calcite acting as a flux [5]. Depending upon the firing conditions, glass phases may also be produced and some of the organic temper may be oxidized into carbon dioxide, or remain in the ceramic in a reduced graphite-like state. The phases formed at high temperatures are not stable at ambient temperatures and pressures, and once buried in the sediment, where they may be exposed to wet or humid conditions and soluble salts, may undergo diagenetic changes with time [6,7].

Irrespective of the production conditions, the burial environment and the duration of burial, the macroscopic appearance of most archaeological sherds, as well as their brittle mechanical properties, appear unchanged. It is well established, however, that the pseudo-amorphous clay mineral components of ceramics do undergo slow rehydration (also referred to as rehydroxylation)

once buried [8–10]. Following Hamilton and Hall [8], we refer to rehydroxylation of the clay minerals as the process involving molecular water reacting to form hydroxyl groups bonded directly to the ceramic mineral matrix.

The pioneering studies of Picon, Buxeda, and Mommsen and colleagues, as well as many follow-up studies, clearly showed that at microscopic levels some sherds undergo diagenetic changes in addition to rehydroxylation [6,11,12]. These changes can include filling of the voids by authigenic newly formed minerals [13], crystallization of glass phases including the formation of the sodium-rich zeolite, analcime (analcite) [11], and at the elemental level losses or changes in the concentrations of various elements [12]. These changes are of interest in themselves, and may also affect the results of ceramic provenience studies based on elemental analyses and textures [7,11].

It has also been established that the ceramics that are most susceptible to diagenetic changes are those that are formed at relatively high temperatures [14]. The amount of analcime that forms also increases with increasing firing temperatures [11]. Ceramics formed at high temperatures contain a larger proportion of mineral/glass components that are more disordered and hence more likely to undergo diagenetic changes.

Here we report an occurrence of sherds in which the pseudo-amorphous clay components of the ceramic have undergone not only rehydroxylation, but also recrystallization and have lost their brittle mechanical properties. In contrast to rehydroxylation, recrystallization of the clay minerals involves transformation of the disordered smectite clay minerals in the ceramics back to crystalline clays, similar to those found in sediments and soils. This transformation occurred in the firing chamber of a Late Byzantine kiln identified and characterized at the site of Tel Qatra (Gedera, Israel) [15].

The study of the section through this kiln, and proof that this was indeed a kiln and not a waste dump, is described in Weiner et al. [15]. Figure 1 shows the section through the kiln with the collapsed pottery chamber at the top, and the firing chamber at the bottom. The pottery chamber is filled with broken vessels. The pottery types in the upper chamber were composed mostly of Gaza-type storage jars (also known as Late Roman Amphora 4), which were used as containers for wine marketing produced in the southern coast of Israel between the Late Roman and Umayyad period [15]). Many of the pieces are still joined indicating that they were broken in situ. The firing temperature of these ceramics was estimated to be around 600 °C based on infrared spectrometry [15]. The firing chamber is located below the pottery chamber. The firing chamber was filled with a fine powdery grey colored ash that is composed mainly of partially melted silica phytoliths and the high temperature mineral cristobalite. Interspersed in the ash is a layer of flattish sherds, which were arranged in antiquity to form a U-shaped surface in the firing chamber. These sherds are clearly fragments of the pottery produced in the kiln and then re-used to form the surface. The round stone-lined structure in the foreground and the intrusive pit are younger features that were dug into the section. The focus of this study is on this layer of sherds.

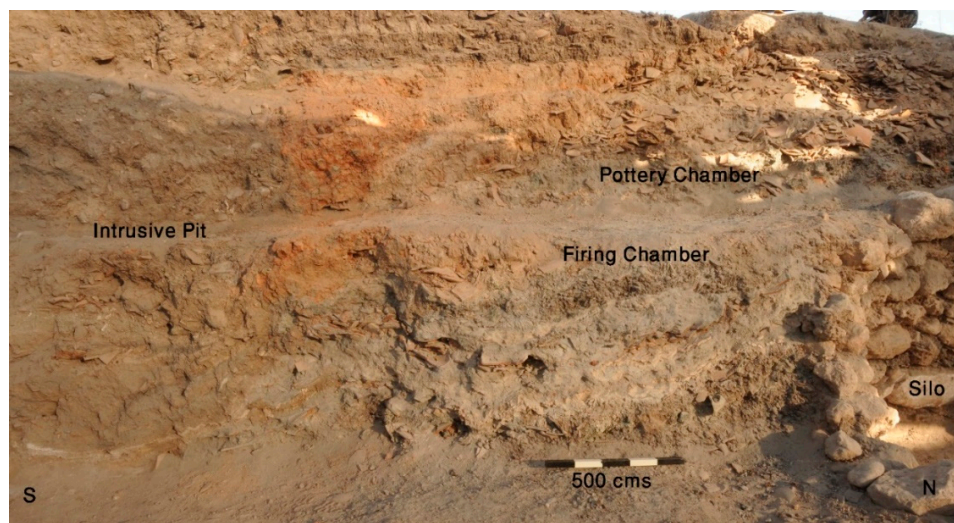


Figure 1. Photograph of the section through the kiln, with the pottery chamber located above the firing chamber. The pit and the silos are intrusive features. The pit has been dated to the Mamluk period some 600 years after the kiln was in operation in the 7th Century CE [15].

2. Materials and Methods

2.1. Materials

Six samples were studied in detail: two pottery sherds from the pottery chamber (sample 514-1 and 514-3). Based on their infrared patterns, sherd 1 was fired at a higher temperature than sherd 3, as the main absorption peak of sherd 1 has an additional higher wavenumber component compared to sherd 3 (data not shown). Four samples were analyzed from the sherd layer in the firing chamber. Their locations are shown in Figure 2. Sherds 563 and 564 are located on the northern side of the firing chamber. They have a dark color and are brittle. Sherds 569 and 570 are in the center of the firing chamber and are light brown-tan colored and very friable.



Figure 2. *Cont.*



Figure 2. (a) Photograph of the layer of sherds in the firing chamber. The layer is embedded in grey sediment that is rich in melted phytoliths, cristobalite, and small amounts of highly disordered calcite [15]. The numbers show the locations of the samples analyzed. (b) Higher magnification view of the central part of the sherd layer showing the transition from dark brittle sherds in the north to light tan colored friable sherds further south. The location of sample 569 is shown.

2.2. Petrography

Fragments from samples 563 and 570 were embedded in EpoFix according to the manufacturer's instructions (Struers, Cleveland, OH, USA). The samples were baked for 2 days at 60 °C and were then glued to a glass slide and cut using a Brilliant 220-ATM saw (Mammelzen, Germany). The slices were then thinned to around 30 µm using the Pot Wheel and a 54-µm grinding powder. The thin sections were examined using a Nikon Eclipse E600 Pol petrographic microscope (Nikon Instruments Inc, Mellville, New York, NY, USA).

Fractions of all 6 samples were lightly ground using a large ceramic mortar and pestle and then passed through a 500 µm sieve. The fraction that did not pass through the sieve was reground and sieved again until almost all the material passed through the sieve. These fractions were used for the following analyses:

2.3. Fourier Transform Infrared Spectroscopy (FTIR)

About 500 micrograms of <500 µm fraction was lightly ground in an agate mortar and pestle and then mixed with 2–3 mg of spectro-grade pure KBr. The mixture was pressed into a 5 mm pellet using a Pike handpress (KBR Pellet Prep, Shimadzu, Scientific Instruments, Columbia, MD, USA). The infrared spectrum of the transparent pellet was obtained using a Nicolet iS5 spectrometer (The Thermo Scientific, Waltham, MA, USA) at 4 cm⁻¹ resolution in the range of 4000 to 400 cm⁻¹.

2.4. X-Ray Powder Diffraction

About a gram of the <500 µm fraction were used for the powder patterns. The measurements were carried out in reflection geometry using a TTRAX III (Rigaku, Tokyo, Japan) diffractometer equipped with a rotating Cu anode operating at 50 kV and 200 mA and with a scintillation detector aligned at the diffracted beam after a bent Graphite monochromator; 2θ/θ scans. The measurements were performed at specular conditions in Bragg–Brentano mode with variable slits and scanned with step size of 0.02° and scan speed of 0.5° per minute, starting from 4° 2θ/θ until above 50°. Phase analysis was made using the Jade 2010 software (Materials Data, Inc., Livermore, CA, USA) and PDF-4+ 2019 database, International Centre for Diffraction Data (ICDD, Newtown Square, OA, USA).

2.5. SEM and EDS

An aliquot from each of the <500 µm fraction was pressed into a 5 mm diameter pellet using a Pike Handpress that applies approximately 2 atmospheres of pressure. Pressure was applied for about 1 min. The pellet was then pressed out of the stainless steel template using a plunger. SEM

images were obtained using a Zeiss Sigma 500 FE-SEM (ZEISS, Oberkochen, Germany) with an Everhart-Thornley detector and a 4QBSD (4-quadrant backscattered electron) detector at landing voltage of 20 kV. The working distance was about 7–8 mm. Energy Dispersive Spectroscopy (EDS) data were collected using a Bruker XFlash® 6|60 detector (Bruker, Billerica, MA, USA) with a 30 mm aperture. The XFlash® 6|60 detector silicon drift detector has an excellent resolution <130 eV. All spectra were fitted in Bruker's Esprit software () by standard procedure using a P/B-ZAF model. All peaks are well resolved and each spectrum was collected with good signal to noise ratio ($\sim 250 \times 10^3$ counts in the complete spectrum) and phase size exceeded X-ray range, which is estimated to be $\sim 2.5 \mu\text{m}$ in radius and $\sim 4 \mu\text{m}$ in depth. As a result, the error of the analysis was <0.5% for Na.

3. Results

Figure 2a is a view of northern part of the firing chamber showing the surface composed of re-used sherd fragments. The northern-most sherds are dark red-brown in color and are extremely brittle. The sherds in the same layer change color to the south to become light brown-tan and they lose their brittleness and have the texture of compressed powder. The locations of the four samples analyzed are shown in Figure 2a. Figure 2b is a close up view of the sherd surface that shows that the sherds in the same layer have changed color becoming light tan towards the south. A few of the sherds are both dark brown in some parts, and light tan in other parts.

In order to gain an initial insight into possible changes that account for the marked differences in mechanical properties and color of the sherds in the firing chamber, we prepared thin sections of the dark brittle sherd 563 and the crumbly light brown-tan colored sherd 570 (Figure 3). Figure 2a shows their locations in the firing chamber. The proportions of sand-sized mainly angular quartz grains to the fine silt-sized matrix are clearly different in the different samples, but we noted that the proportions vary considerably in different areas of the slides in both specimens. A high proportion of dark red ferruginous material is present in 563, but is almost absent in 570. This reflects the visible differences in color (Figure 2). The matrices of both samples are composed of fine-grained calcite and clay. The calcite components in both samples are birefringent and hence crystalline. The presence or absence of clay birefringence in both samples cannot be discerned in crossed polarized light, even at higher magnifications.

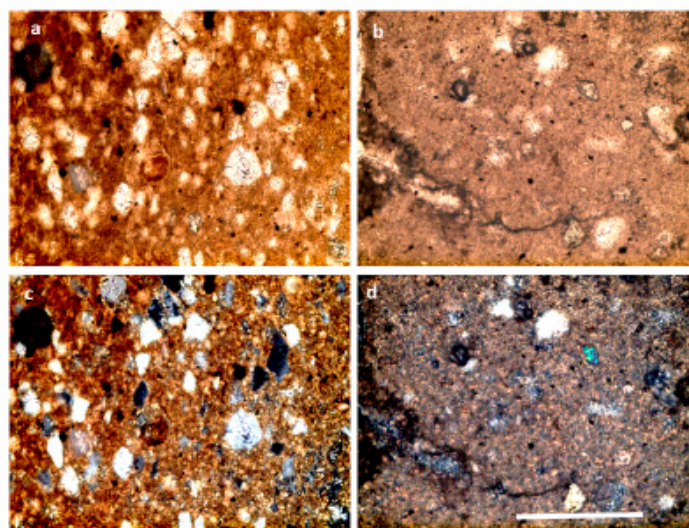


Figure 3. Optical light microscope images of samples 563 (a,c) and 570 (b,d). Plain polarized light was used for images a and b, and crossed polarized light for images c and d. The sand-sized large angular inclusions are mostly quartz. The fine-grained silt-sized matrix of 563 has abundant ferruginous material giving the sample a reddish dark color, whereas this ferruginous material is absent in 570. The fine-grained matrix is composed of calcite, which is birefringent, and clay minerals. The crack in sample 570 has been filled in with secondary calcite. All images are at the same magnification. Scale bar is 250 μm .

For the spectroscopic and chemical analyses, we lightly ground all the samples and used only the fraction that was less than 500 μm . We also avoided exposing the samples to any solvents including water, as we did not want to risk having the more disordered and hence more soluble mineral components dissolving.

Figure 4 shows the FTIR spectra of the <500 μm fractions from sherds 563, 564, 569, and 570 (Figure 2) and for comparison, the spectra of 2 sherds from the pottery chamber above (514-1 and 514-3). The figure also shows the spectrum of sediment from the local stream/wadi of Nahal Soreq less than a kilometer from the site. The major mineral components of all the samples are calcite, clay minerals, and quartz (see legend of Figure 4). Spectrum 563 is very similar to the sherds from the upper chamber, whereas spectra 569 and 570 are very similar to the local wadi sediment. Spectrum 564 is intermediate between the two groups. This most surprising result shows that even though 569 (and to some extent 570) still have the shapes of sherds (Figure 2b), their clay component is crystalline as opposed to the disordered smectite in the sherds from the upper chamber. This is deduced from the facts that the IR spectra of samples 569 and 570 contain not only the hydroxyl peaks 3696 and 3619 cm^{-1} indicating rehydroxylation, but their major peaks have shifted from around 1080–1050 cm^{-1} in the ceramic samples (due to the absorption of the pseudo-amorphous clay [4]) to 1032 cm^{-1} , which is a characteristic absorption of the local clay minerals. The Si–O–Si peak at 515 cm^{-1} is also present in 569 and 570, but absent in the ceramic spectra. The spectra of the altered sherds 569 and 570 are almost identical to sediment from the local stream (wadi) of Nahal Soreq, located less than a kilometer from the site. Clearly, the clay components of sherds 569 and 570 in the firing chamber have recrystallized.

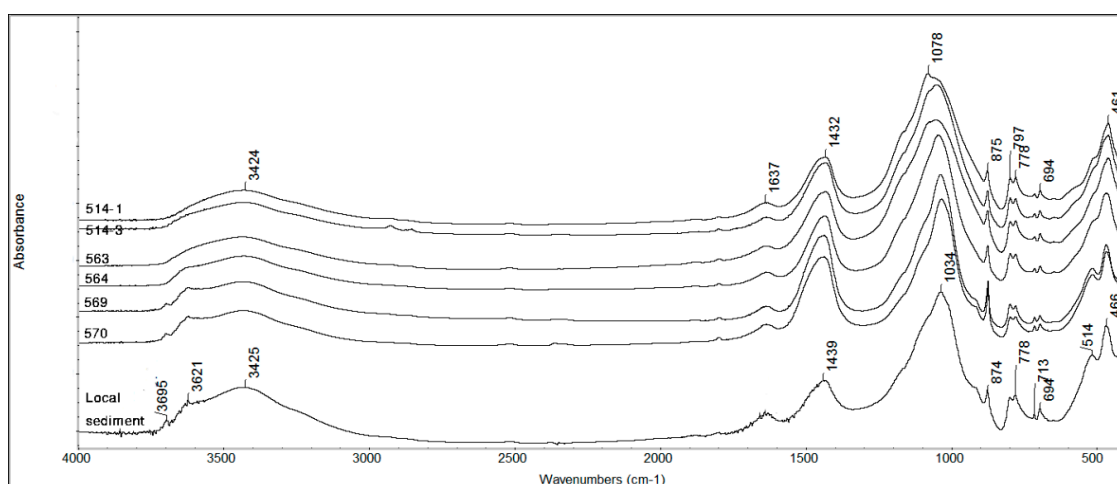


Figure 4. Infrared spectra of the 6 <500 μm samples from the upper pottery chamber (514-1 and 514-3) and the sherd layer in the lower firing chamber (from north to south: 563, 564, 569, and 570 (see Figure 2a)). The spectrum of sediment from the local wadi is also shown. The peaks for calcite are 1430, 875, and 713 cm^{-1} . The unique peak for quartz is at 694 cm^{-1} . The unique peaks for crystalline clay mineral are the hydroxyl groups at 3695 and 3621, the shoulder at 912 and the Si–O–Si peak at 514 cm^{-1} . The absence of the hydroxyl peaks and the 514 peak in the ceramics, and the shift of the main peak in the ceramics to higher wavenumbers compared to crystalline clay, all attest to the presence of disordered clay mineral in the ceramics that have not undergone recrystallization. The presence of the peaks of crystalline clay in sherds 569 and 570, and in the local sediment, attest to the presence of crystalline clay mineral.

Figure 5 shows the powder X-ray diffraction patterns of the 6 <500 μm powder samples: two sherds from the upper chamber (514-1 and 514-3), two dark sherds (563 and 564) and two light tan colored soft and friable sherds (569 and 570) from the firing chamber (Figure 2). All the samples contain quartz (Q), calcite (C), cristobalite (Cr), and montmorillonite (M). Significantly the montmorillonite main peak at around 20° 2-theta is particularly prominent in the two recrystallized sherds, 569 and 570,

compared to the other samples. Furthermore, both 569 and 570 contain kaolinite peaks (e.g., peak at 12.3° 2-theta), whereas the other samples do not. We therefore conclude that during the recrystallization process, more crystalline montmorillonite formed and kaolinite formed de novo. The prominent baseline rise in the region of $4\text{--}10^\circ$, 2-theta is present only in samples 569 and 570. We suspect that this is due to the presence of closely related phases of montmorillonite that comprise relatively disordered small crystallites that bind varying amounts of water.

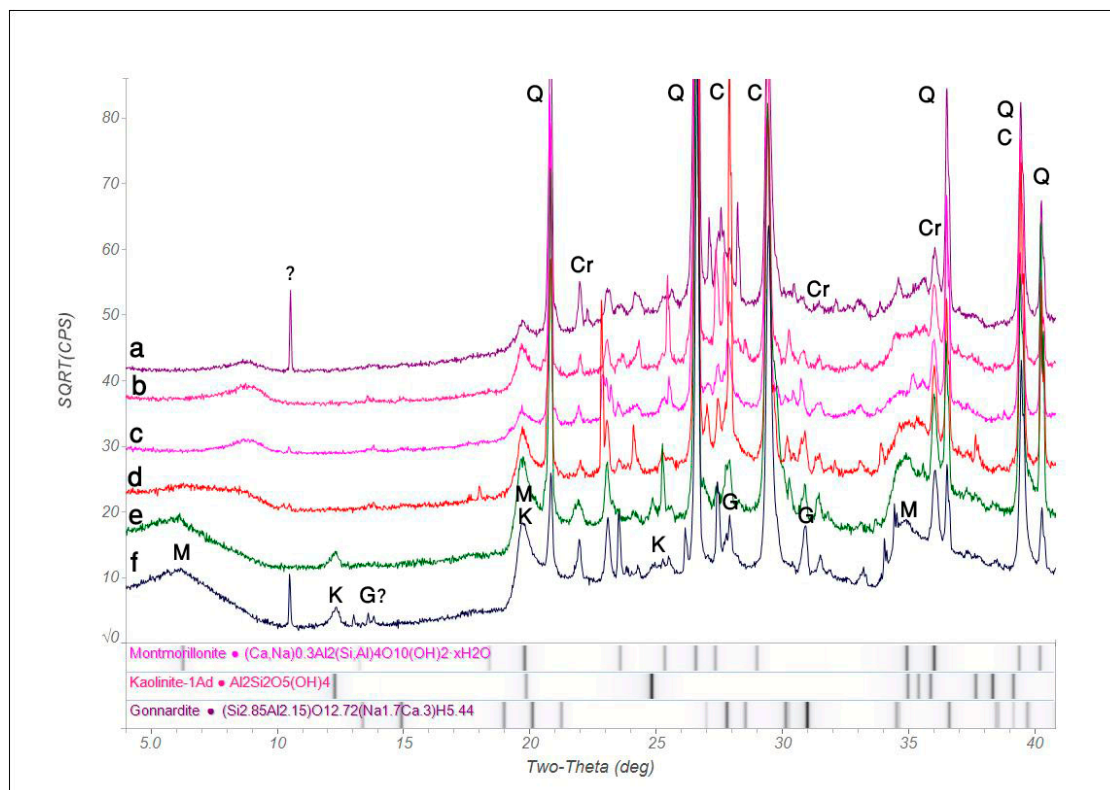


Figure 5. X-ray powder diffraction spectra of the 6 samples: (a) 514-1, (b) 514-3, (c) 563, (d) 564, (e) 570 and (f) 569. The spectra are shown as recorded, and the peak intensities have not been normalized. Thus, the peak heights approximately reflect the relative proportions of the mineral components, assuming that this is a true powder with no preferred orientations. The strong reflections of the abundant quartz, cristobalite, and calcite minerals are identified on the top spectrum and the strong and non-overlapping reflections of kaolinite, montmorillonite, and gonnardite are identified on spectrum f. For comparison, we also show at the base of the image the reflections of kaolinite, montmorillonite and gonnardite obtained from a reference library (International Centre for Diffraction Data (ICDD), PDF-4+ 2019). Q-quartz 98-000-0369; C-calcite 98-000-0141; M-montmorillonite 00-060-0318; Cr-cristobalite 98-000-0178; K-kaolinite 00-014-0164; G-gonnardite 98-000-3619.

Sample 569 has small peaks that can be assigned to the zeolite gonnardite (Figure 5). Gonnardite may be present in very small amounts in all the other samples, including the two sherds from the pottery chamber. This is consistent with EDS analyses (see below).

The question then arose as to whether or not these, or other zeolites, formed during the recrystallization process or as a result of diagenesis of ceramics that had not undergone recrystallization. Analcime is known to form diagenetically in ceramics heated to high temperatures [11,14]. We therefore decided to map the distribution of sodium in a control sherd from the upper pottery chamber (514-1) and one of the diagenetically altered samples from the center of the firing chamber (569) using EDS in the SEM as many zeolites are characteristically rich in sodium [16]. Figure 6 shows examples of Na maps obtained from the surfaces of samples that were pressed with around 2 tons of pressure for a few

minutes. We deliberately avoided embedding and polishing the samples, as we wanted to avoid the possibility of losing the relatively soft zeolitic minerals, if present, due to polishing.

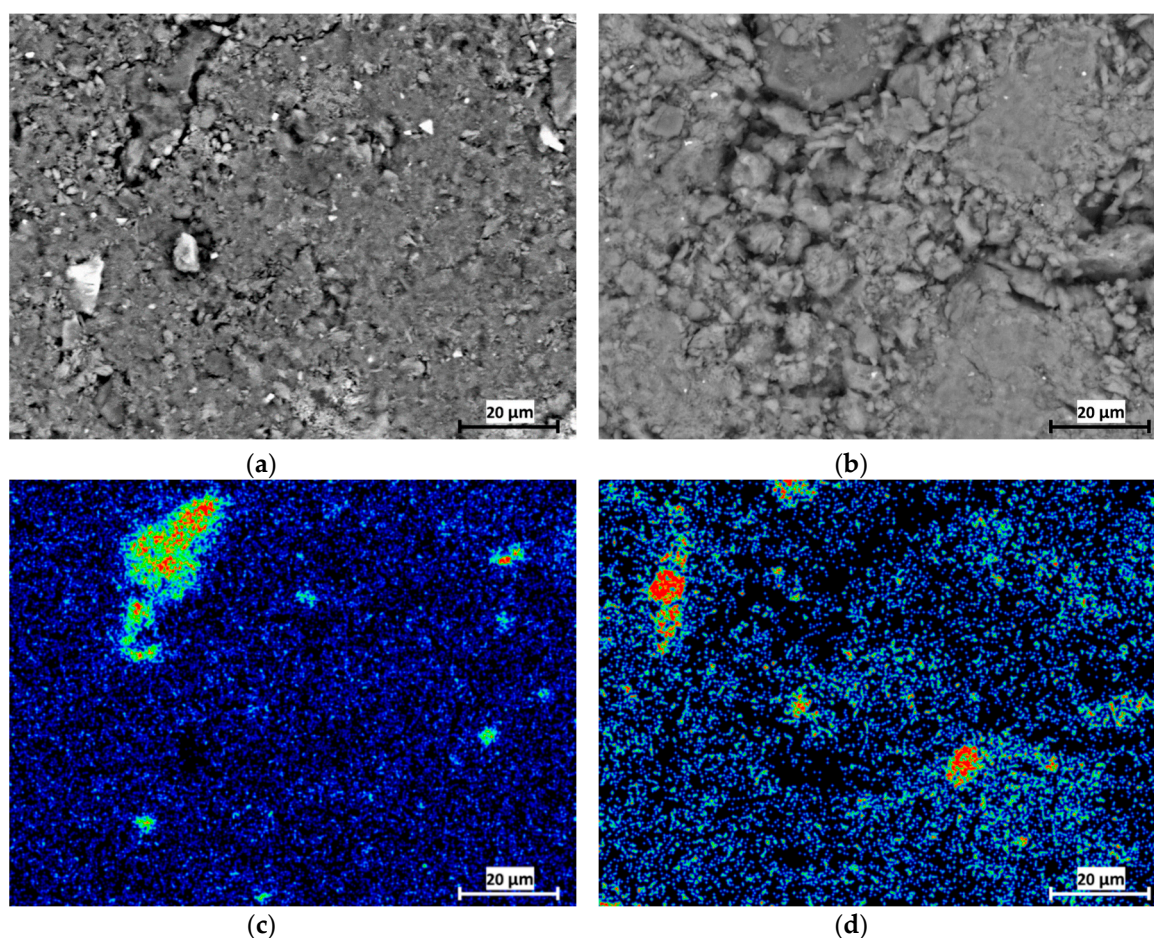


Figure 6. (a) and (b) are backscattered images of sherds 569 and 514-1, respectively; (c) and (d) are energy dispersive X-ray spectroscopy (EDS) maps of Na signal intensity of 569 and 514-1, respectively. Grains with excess of Na can be easily identified.

We analyzed 18 Na-rich grains in 514-1 and 8 Na-rich grains in 569. We arbitrarily divided the grains into 3 groups: (1) Na around 10 atom % or higher; (2) Na around 7 atom %; (3) Na around 5 atom %. Note that the error of these analyses is less than $\pm 0.5\%$. The average elemental analyses and the number of particles in each group are shown in Table 1 for samples 514 and 569. There are no clear-cut differences between the Na-rich particles in sample 514 compared to sample 569. We also note that in almost all the particles the total number of cations (Na, Mg, Ca, Fe, K) is similar to the amount of aluminum. The Si/Al ratios vary from around 2.0 to 2.7. From these observations we can conclude that there are two likely stoichiometries for these Na-rich minerals: $(\text{Na, Mg, Ca, Fe, K})\text{AlSi}_2$ when the Si/Al ratio is around 2, and $(\text{Na, Mg, Ca, Fe, K})_2\text{Al}_2\text{Si}_5$ when the Si/Al ratio is around 2.5. The grains with a stoichiometry of $(\text{Na, Mg, Ca, Fe, K})\text{AlSi}_2$ could have the structure of analcime $(\text{Na}[\text{AlSi}_2\text{O}_6]\cdot\text{H}_2\text{O})$, but where some of the Na is substituted by Ca and other cations. The grains with a stoichiometry of $(\text{Na, Mg, Ca, Fe, K})_2\text{Al}_2\text{Si}_5$ could have the structure of gonnardite $(\text{Na}_2\text{Ca}[(\text{Al,Si})_5\text{O}_{10}]\cdot 6\text{H}_2\text{O})$, and here, too, some of the Na and Ca is substituted by other cations. Such substitutions are known to occur in zeolites [16]. These analyses are consistent with gonnardite being present in sample 569 based on X-ray diffraction and in smaller amounts in other samples.

Table 1. EDS analyses (atom %) of Na-rich grains from samples 514 and 569 arbitrarily divided into three groups (see text) according to their Na atom % values.

Sample	514	514	514	569	569	569
	<i>n</i> = 5	<i>n</i> = 6	<i>n</i> = 7	<i>n</i> = 2	<i>n</i> = 5	<i>n</i> = 1
Group	1	2	3	1	2	3
Na	11.44	7.40	5.40	9.50	7.03	5.06
Mg	0.16	0.36	0.61	0.35	0.86	0.32
Ca	4.22	6.33	6.72	2.22	4.56	7.79
Fe	0.47	0.79	1.30	0.54	1.18	0.85
K	0.24	0.59	0.59	0.10	0.6	0.67
Si	37.63	37.65	38.16	40.34	42.46	35.51
Al	17.79	15.39	17.53	14.70	16.27	19.50
Na, Mg, Ca, Fe, K	16.53	15.47	14.62	12.71	14.23	14.69
Si/Al	2.12	2.45	2.18	2.74	2.61	1.82

4. Discussion

Here we show that the pseudo-amorphous clay components of some of the low-fired ceramics that were re-used to form a surface in the firing chamber of a pottery kiln have transformed into crystalline clay minerals. This is presumably because they were exposed to high temperatures in the firing chamber. The recrystallized clay minerals are mostly montmorillonite, as well as kaolinite. We also identified zeolite minerals. These zeolites are also present in ceramics from the upper pottery chamber of the kiln that have not recrystallized.

Rehydroxylation of disordered clay minerals in a ceramic is a well-known phenomenon [8]. The rehydroxylated clay minerals however generally remain disordered. Here we demonstrate that the pseudo-amorphous clay minerals in the ceramics of the firing chamber have not only undergone rehydroxylation, but have also recrystallized and reverted back to crystalline clays. Montmorillonite is the dominant crystalline clay in the recrystallized ceramic. Smectites (including montmorillonite) are also the most common clay type found in the local sediments of the coastal plain of Central Israel [17]. The powder X-ray diffraction patterns show that the montmorillonite in the recrystallized ceramics is also more abundant than in the other four samples analyzed. Thus, some of the montmorillonite in the recrystallized ceramics, as well as the kaolinite, which was only present in the recrystallized ceramics, are authigenic minerals that formed during the recrystallization process. It is significant that this recrystallization occurred mainly in the ceramics in the center of the firing chamber where the temperature was presumably the highest. Furthermore, being a firing chamber, these ceramics were presumably subjected to repeated high temperature firing events.

The ash above and below the ceramic surface comprises mainly melted phytoliths and at some locations, even phytolith-derived slags [15]. Furthermore, the ash contains cristobalite, a high temperature silicate mineral that generally forms above 600 °C when phytoliths are heated [18]. We also identified cristobalite in the recrystallized and non-recrystallized ceramics from the firing chamber and the upper pottery chamber. It is surprising that the two sherds from the upper pottery chamber also contained cristobalite, as we would not expect this high temperature mineral to form in the ceramic itself unless it was derived from the devitrification of opal (silica) [19]. This opal may be from ash phytoliths that do contain cristobalite [15] and were somehow occluded in the ceramics. If, however, the cristobalite in the ceramics formed at very high temperatures, it is conceivable that these temperatures occurred during an over firing event that resulted in the collapse of the kiln.

Kingery carried out differential thermal analysis (DTA) of ceramics of archaeological pottery specimens, and identified some which had a DTA pattern similar, but not identical to unfired clay minerals [20]. He proposed that “archaeological ceramic samples originally fired at below 700–800 °C re-acquire many of the characteristics of an unfired clay over several millennia (p111).” Capel et al. observed neoformed smectites in the glassy phase of Bronze Age fired pottery [21]. Shoval et al. reported that in Bronze and Iron Age pottery from the southern Levant small amounts of recrystallized

(neoformed or reconstructed) clay minerals may be detected, but the bulk of the clay remains in its amorphous form [22]. In this study, we compare ceramics from the same surface and from the upper and lower chambers of the same kiln. As only those subjected to repeated high temperature events underwent recrystallization, we conclude that the ceramics that were repeatedly exposed to high temperatures were the ones that recrystallized.

The sherds that have been altered diagenetically are light tan-brown in color as opposed to the dark reddish color of the better preserved sherds. The petrographic analysis of the thin sections showed that the ferruginous component has been lost during the extreme diagenesis. The chemical conditions responsible for this loss are not obvious, unless, somehow during the re-firing events, the iron atoms were reduced and, hence, became more soluble. We note that we were unable to detect the presence of recrystallized clay minerals in the petrographic thin sections of sample 570. We suspect that the very small grain size of both the clay minerals and the calcite in the matrix, as well as the fact that the calcite is clearly birefringent, prevented us from discerning the presence of birefringent crystalline clay minerals in the matrix.

It is interesting to note that all six ceramics examined contain calcite. The fact that the ash in which they were embedded also contains cristobalite and was hence heated to relatively high temperatures, implies that the calcite in the firing chamber sherds was probably reformed from hydrated CaO derived from the original calcite [23]. The source of the carbon dioxide could be from the breakdown of the original calcite or from the atmosphere [24]. Thus, the calcite identified in the ceramic samples has a different origin than the calcite identified in the sediments from the nearby stream. Furthermore, the atoms in the calcite are extremely disordered. This extent of disorder is consistent with the ash calcite having been reheated to around 900 °C [23].

Exposure to repeated high temperature events could well occur on the outer surfaces of ceramic cooking pots, whether they were used over an open fire or in an oven. If indeed cooking pots do undergo recrystallization, it could be difficult to detect as the recrystallized clay minerals might be confined to just below the outer surface. In fact, Shoal et al. [22], using FTIR, noted that calcareous cooking pots from the Bronze Age in the southern Levant do have small amounts of recrystallized (reconstructed) clay minerals. Thus, clay recrystallization might well affect provenience studies based on elemental analyses of entire ceramic sherds, as recrystallization is likely to affect the elemental composition. Moreover, this might be particularly relevant to provenience studies involving cooking pots.

We identified the presence of the zeolite gonnardite in the ceramics from both the upper chamber and from the firing chamber using X-ray diffraction. The presence of analcime and gonnardite is consistent with the EDS analyses (Al:Si = 1:2 and 1:2.5 respectively). The EDS analyses shows that some of the Na is substituted by Ca and other cations. The gonnardite seems to be present in all six samples analyzed by X-ray diffraction, albeit in larger amounts in the recrystallized samples (569 and 570). The presence of these zeolites in “normal” ceramics from the pottery chamber and the recrystallized ceramics indicates that their formation is not dependent upon repeated exposure to high temperature events, but as has been proposed, it is dependent on diagenesis of most probably the less ordered glassy phases of the ceramics. This process has been well documented [6,11].

5. Conclusions

Infrared spectrometry shows that the clay minerals in two ceramic sherds that were used to form a surface in the firing chamber of a Late Byzantine kiln have undergone almost complete recrystallization. The infrared spectra of these recrystallized sherds closely resemble the spectrum of the sediments from the local stream. Authigenic montmorillonite and kaolinite formed during the recrystallization process. The zeolite gonnardite was identified by X-ray diffraction and EDS, and the presence of analcime was inferred from EDS. These zeolites however were present in all the samples examined and, therefore, did not form only as a result of the recrystallization process. Pseudo-amorphous clay recrystallization in these ceramics was probably a result of repeated exposure to high temperatures. We can, thus, infer that recrystallization may well occur beneath the outer surfaces of cooking pots that are also subjected

to repeated exposure to high temperatures and, if so, could well affect provenience studies based on elemental analyses involving cooking pots.

Author Contributions: S.W., Y.F. and A.K. all participated in the data analysis and writing of the manuscript. A.N. directed the excavation. All authors have read and agreed to the published version of the manuscript

Funding: This research was in part funded by the Kimmel Center for Archaeological Science of the Weizmann Institute of Science.

Acknowledgments: We thank Iddo Pinkas, Weizmann Institute of Science, for his help in this project, as well as Filipe Natalio, Weizmann Institute of Science, for preparing the thin sections. We also thank Louise Gomart for her critical reading of the manuscript and valuable suggestions.

Conflicts of Interest: The authors declare no conflict of interest.

References

1. Rapp, G.R. *Archaeomineralogy*; Springer: Heidelberg, Germany, 2002.
2. Livingstone Smith, A. Bonefire II: the return of pottery firing temperatures. *J. Archaeol. Sci.* **2001**, *28*, 991–1003. [[CrossRef](#)]
3. Whitbread, I.K. Ceramic petrology, clay geochemistry and ceramic production—From technology to the mind of the potter. In *Handbook of Archaeological Sciences*; Brothwell, D.R., Pollard, A.M., Eds.; John Wiley & Sons: Chichester, UK, 2001; pp. 449–459.
4. Shoval, S.; Paz, Y. Analyzing the fired-clay ceramic of EBA Canaanite pottery using FT-IR spectroscopy and LA-ICP-MS. *Period. Mineral.* **2015**, *84*, 213–231.
5. Kingery, W.D.; Bowen, H.K.; Uhlmann, D.R. *Introduction to Ceramics*; John Wiley & Sons: New York, NY, USA, 1960.
6. Picon, M. Remarques préliminaires sur deux types d'altération de la composition chimique des céramiques au cours du temps. *Figlina* **1976**, *1*, 159–166.
7. Schwedt, A.; Mommsen, H.; Zacharias, N. Post-depositional elemental alterations in pottery: Neutron activation analyses of core and surface samples. *Archaeometry* **2004**, *46*, 85–101. [[CrossRef](#)]
8. Hamilton, A.; Hall, C. A review of rehydroxylation in fired-clay ceramics. *J. Am. Ceram. Soc.* **2012**, *95*, 2673–2678. [[CrossRef](#)]
9. Washburn, E.W.; Footitt, F.F. Porosity: III. Water as an absorption liquid. *J. Am. Ceram. Soc.* **1921**, *4*, 527–537. [[CrossRef](#)]
10. Heller, L.; Farmer, V.C.; Mackenzie, R.C.; Mitchell, B.D.; Taylor, H.F.W. The dehydroxylation and rehydroxylation of triphormic dioctahedral clay minerals. *Clay Miner. Bull.* **1962**, *5*, 56–72. [[CrossRef](#)]
11. Buxeda, J.; Garrigós, I.; Mommsen, H.; Tzolakidou, A. Alterations of Na, K and Rb concentrations in Mycenaean pottery and a proposed explanation using X-ray diffraction. *Archaeometry* **2002**, *44*, 187–198. [[CrossRef](#)]
12. Buxeda, J.; Garrigos, I.; Kilikoglou, V.; Day, P.M. Chemical and mineralogical alterations of ceramics from a Late Bronze Age kiln at Kommos, Crete: the effect on the formation of a reference group. *Archaeometry* **2001**, *43*, 349–371.
13. Maritan, L.; Mazzoli, C. Phosphates in archaeological finds: implications for environmental conditions of burial. *Archaeometry* **2004**, *46*, 673–683. [[CrossRef](#)]
14. Schwedt, A.; Mommsen, H.; Zacharias, N.; Buxeda, J.; Garrigos, I. Analcime crystallization and compositional profiles—Comparing approaches to detect post-depositional alterations in archaeological pottery. *Archaeometry* **2006**, *48*, 237–251. [[CrossRef](#)]
15. Weiner, S.; Nagorsky, A.; Taxel, I.; Asscher, Y.; Albert, R.M.; Regev, L.; Yan, X.; Natalio, F.; Boaretto, E. High temperature pyrotechnology: A macro- and microarchaeology study of a Late Byzantine-beginning of Early Islamic period (7th century AD) pottery kiln from Tel Qatra/Gedera, Israel. *J. Archaeol. Sci. Rep.* **2020**. [[CrossRef](#)]
16. Deer, W.A.; Howie, R.A.; Zussman, J. *An Introduction to the Rock-Forming Minerals*; London Scientific and Technical: London, UK, 1992.
17. Stanley, D.J.; Mart, Y.; Nir, Y. Clay mineral distributions to interpret Nile cell provenance and dispersal: II. Coastal plain from Nile Delta to Northern Israel. *J. Coast. Res.* **1997**, *13*, 506–533.

18. Hammad, M.A.; Khattab, I.A. Effect of the combustion process on the structure of rice hull silica. *Thermochim. Acta* **1981**, *48*, 343–349. [[CrossRef](#)]
19. Gualtieri, A.; Bertolani, M. Mullite and cristobalite formation in fired products starting from halloysitic clay. *Appl. Clay Sci.* **1992**, *7*, 251–262. [[CrossRef](#)]
20. Kingery, W.D. A note on the differential thermal analysis of archaeological ceramics. *Archaeometry* **1974**, *16*, 109–112. [[CrossRef](#)]
21. Capel, J.; Huertas, F.; Linares, J. High temperature reactions and use of Bronze Age Pottery from La Mancha, Central Spain. *Mineral. Petrogr. Acta* **1985**, *29*, 563–575.
22. Shoval, S.; Beck, P.; Kirsh, Y.; Levy, D.; Gaft, M.; Yadin, E. Rerhydroxylation of clay minerals and hydration in ancient pottery from the “Land of Geshur”. *J. Therm. Anal.* **1991**, *37*, 1579–1592. [[CrossRef](#)]
23. Shoval, S.; Graft, M.; Beck, P.; Kirsh, Y. Thermal behavior of limestone and monocrystalline calcite tempers during firing and their use in ancient vessels. *J. Therm. Anal.* **1993**, *40*, 263–273. [[CrossRef](#)]
24. Shoval, S.; Yofe, O.; Nathan, Y. Distinguishing between natural and recarbonated calcite in oil shales. *J. Therm. Anal. Calorim.* **2003**, *71*, 883–892. [[CrossRef](#)]



© 2020 by the authors. Licensee MDPI, Basel, Switzerland. This article is an open access article distributed under the terms and conditions of the Creative Commons Attribution (CC BY) license (<http://creativecommons.org/licenses/by/4.0/>).